Safe-by-design gelatin modified zinc oxide nanoparticles

Željko Janićijević[1,2*], Ana Stanković[2], Bojana Žegura[3], Đorđe Veljović[4], Ljiljana Djekić[5], Danina Krajišnik[5], Metka Filipič[3], Magdalena Stevanović[2]

[1]*University of Belgrade, School of Electrical Engineering, Bulevar kralja Aleksandra 73, 11120 Belgrade, Serbia*

[2]*Institute of Technical Sciences of SASA, Knez Mihailova 35/IV, 11000 Belgrade, Serbia*

[3]*Department of Genetic Toxicology and Cancer Biology, National Institute of Biology, Večna pot 111, 1000 Ljubljana, Slovenia*

[4]*University of Belgrade, Faculty of Technology and Metallurgy, Karnegijeva 4, 11120 Belgrade, Serbia*

[5]*Department of Pharmaceutical Technology and Cosmetology, University of Belgrade - Faculty of Pharmacy, Vojvode Stepe 450, 11221 Belgrade, Serbia*

*Corresponding author

Dr. Željko Janićijević

E-mail address: zeljkoj@etf.bg.ac.rs

ORCID: 0000-0002-9494-9529

Abstract

We report an innovative low-cost wet precipitation synthesis method for gelatin modified zinc oxide nanoparticles (GM ZnO NPs) at the interface between the gelatin hydrogel and aqueous electrolyte.

Diffusion of ammonia through the hydrogel matrices with different gelatin content induced precipitation of the product in contact with the surface of the aqueous solution of zinc ions. The obtained precipitate was subjected to thermal treatment to partially decompose the adsorbed gelatin in the NP structure. Physicochemical properties of obtained GM ZnO NPs were characterized by X-ray powder diffraction (XRD), scanning electron microscopy (SEM), Fourier-transform infrared spectroscopy (FTIR), differential thermal analysis (DTA), thermogravimetry (TG), photon correlation spectroscopy (PCS), zeta potential measurements, and inductively coupled plasma-mass spectrometry (ICP-MS). The estimated mean crystallite size of GM ZnO NP powders was in the range from 5.8 nm to 12.1 nm. The synthesized NPs exhibit nanosheet morphology and arrange into flake-like aggregates. The toxic potential was investigated *in vitro* in human hepatocellular carcinoma cell line HepG2. The thiazolyl blue tetrazolium bromide (MTS) assay was used to assess cell viability, 2',7'-dichlor-fluorescein-diacetate (DCFH-DA) assay to examine the formation of intracellular reactive oxygen species (ROS), and comet assay to evaluate the genotoxic response. GM ZnO NPs slightly reduced HepG2 cell viability, did not induce ROS formation, and showed low genotoxic potential at very high doses (100 μg mL^{-1}). ZnO NPs fabricated and modified using the proposed methodology deserve further study as potential candidates for antibacterial agents or dietary supplements with low overall toxicity.

Keywords

ZnO, nanoparticles, precipitation, gelatin, hydrogel, toxicity

Acknowledgments

We thank Dr. Ljiljana Veselinović from the Institute of Technical Sciences of SASA for the acquisition of XRD spectra. We also acknowledge the support of the funding sources: the Ministry of Education, Science and Technological Development of the Republic of Serbia (Agreement on realization and financing of scientific research work of the Institute of Technical Sciences of SASA in 2020 (Record number: 451-03-68 / 2020-14 / 200175)), COST Action CA15114, the bilateral collaboration between Serbia and Slovenia (BI-RS/16-17-039), and Slovenian Research Agency: Program P1-0245).

1. Introduction

Zinc oxide (ZnO) is a multifunctional material used for diverse applications in fields such as biomedicine, photonics, electronics, cosmetics, the food industry, and many others. Nanostructured ZnOs are highly promising materials for a variety of biomedical applications including antibacterial, antidiabetic, and anticancer agents, biosensing, biomedical imaging, drug and gene delivery, wound healing, etc [1–4]. ZnO in the form of nanoparticles (NPs) has also proved to be beneficial for improving dietary supplementation [5, 6].

Various synthesis methods were designed and developed for the production of ZnO NPs to achieve suitable material properties and address specific applications [7, 8]. In their previous studies, Stanković et al. (2013, 2016) demonstrated the possibility to significantly alter the morphology and average particle size of ZnO by changing the pH value of the reaction system in hydrothermal processing, as well as the successful preparation of ZnO NPs via a simple microwave-assisted synthesis method. Among many synthesis methods, wet chemical precipitation stands out as a simple and low-cost method, which is easily modified and suitable for large-scale fabrication. Many studies have been performed to optimize the precipitation synthesis protocols by varying the physical parameters, precursors, stabilizers, and composition of the synthesis medium [11–22].

Several attempts have been made to modify the precipitation of ZnO NPs in the presence of gelatin as a biologically derived and highly biocompatible material. These studies were mainly focused on the precipitation in gelatin solution where gelatin can act as a stabilizer and organic template for nucleation and crystallization of ZnO NPs [23–29]. However, one of the studies also reports the possibility of using immobilized gelatin on the silicon wafer surface to modify ZnO crystallization [23].

Although ZnO NPs exhibit a multitude of favorable properties, their use in biomedicine is often hampered by the issue of toxicity, which is still not completely understood. Four different main mechanisms are commonly proposed in the literature (see [30–32] and references therein, and also [33–37]): 1) direct contact of ZnO NPs with the cell surface structures destroying the structural integrity of cells, 2) ZnO dissolution

and shedding of Zn^{2+} ions, 3) generation of reactive oxygen species (ROS), and 4) cellular internalization of ZnO NPs.

The generation of ROS is commonly considered the most important mechanism and main contributor to ZnO NP toxicity [32]. However, the importance of other mechanisms cannot be neglected (e.g. involving the disruption of the cell membrane and leakage of cell contents) [38]. Some findings also imply that more meticulous research is required at the molecular level to unravel the underlying toxicity mechanisms that may involve several metabolic pathways [39].

The potential of ZnO NP to induce toxicity depends on the physical, chemical, and biological parameters described in the literature [32, 40, 41]. Toxicity of ZnO NPs is influenced by many factors including particle size and morphology [9, 42–44], particle concentration [45–47], particle surface properties [48, 49], particle interfacial potential [50], cell type [51, 52], medium composition [53], and pH [54–56].

ZnO NPs typically exhibit higher toxicity towards bacterial and cancerous cells compared to normal human cells [51, 57–59]. However, cytotoxic and genotoxic effects of ZnO NPs on normal human cells reported in the literature [59–62] should also be minimized to achieve safe and effective treatment. There were only few attempts to reduce the toxicity of ZnO NPs using the approaches of transitional metal doping [63, 64], silica coating [65, 66], and other surface chemistry modifications [67–72].

Most notable metal doping with iron decreased ZnO NP dissolution and release of Zn^{2+} ions, but it also increased ROS generation (probably through Fenton-type reactions), and overall toxicity was not reduced [64]. Hermetic silica coating of ZnO nanorods reduced their genotoxicity [65], while another study showed reduced cytotoxicity of silica-coated ZnO NPs through the decrease in the dissolution of core ZnO NPs [66]. Surface chemistry was found to influence the generation of ROS directly [67], and the PEGylation of ZnO NPs contributed to the reduction in cytotoxicity through the decrease in cellular uptake [69]. Decomposition of organic impurities at the surface of commercial ZnO NPs with hydrogen peroxide treatment also led to the reduced cytotoxicity attributed to decreased ROS generation and protection of membrane integrity [70]. Synthesized ZnO NPs were also precoated by incubation in the supplemented medium for cell culture to induce the formation of the hard protein corona, which in turn significantly lowered their toxicity. The

approach used in this study led to the inhibition of ROS generation as well as to the reduced dissolution of ZnO NPs [71]. Coating of ZnO nanocrystals with 2-(2-methoxyethoxy)acetate ligand shell prevented the release of Zn^{2+} ions from the core and inhibited ROS generation [72].

Further improvements in the fabrication of ZnO NPs are necessary to produce safe nanomaterials for diverse biomedical applications. The issue of nanomaterials safety becomes increasingly important not only from the biomedical but also from the environmental perspective implying that new nanomaterials should be safe by design [73–75].

We present an innovative precipitation synthesis of gelatin modified (GM) ZnO NPs at the gel/liquid interface where NP properties can be modulated by changing the gelatin content of the hydrogel. Our synthesis methodology results in altered ZnO NPs which are safe-by-design with very low *in vitro* toxicity.

2. Materials and methods

2.1. Materials

Synthesis of GM ZnO NPs was performed using the following chemicals: zinc acetate dihydrate ($Zn(CH_3COO)_2 \cdot 2H_2O$) p.a. purchased from E. Merck, Darmstadt, Germany, edible bovine gelatin (crystal, ~220 g Bloom) obtained from Delhaize Group, and 25% aqueous ammonia solution (NH_4OH) p.a. supplied by NRK Inženjering, Belgrade, Serbia. All chemicals were used without further purification. The aqueous solutions used for the synthesis were prepared with distilled water.

The following chemicals were used for toxicological assessment: Eagle Minimal Essential Medium and fetal bovine serum (FBS) were obtained from Gibco, Life Technologies, Paisley, UK; non-essential amino acids, ethanol, methanol, dimethylsulphoxide (DMSO), phenazine methosulfate (PMS), tert-butyl hydroperoxide (TBHP), benzo(a)pyrene (BaP) from Sigma, St. Louis, MO, USA; penicillin/streptomycin, FBS, L-glutamine and phosphate-buffered saline (PBS) from PAA Laboratories, Dartmouth, NH, USA; etoposide (ET) from Santa Cruz Biotechnology, St. Cruz, USA; low melting point agarose (LMP), normal melting point agarose (NMP), 2',7'-dichlor-fluorescein-diacetate (DCFH-DA) and trypsin from Invitrogen™, Life Technologies, Carlsbad, CA, USA; triton X-100 from Fisher Sciences, New Jersey, USA; thiazolyl blue

tetrazolium bromide (MTS) from Promega (Madison, USA) and GelRed™ from Biotium, Fremont, CA, USA. All other chemical reagents were of the purest grade available, and all solutions were made using Milli-Q water.

2.2. Synthesis of GM ZnO NPs

GM ZnO NPs were synthesized using the modified wet precipitation method at the gel/liquid interface in the open reactor under atmospheric pressure. 0.878 g of $Zn(CH_3COO)_2 \cdot 2H_2O$ was dissolved in 100 mL of distilled water. The required amount of bovine gelatin was mixed with distilled water to obtain 40 g of 5 wt%, 10 wt%, or 15 wt% gelatin solution. The mixture was mildly stirred at a rate of 200 rpm for 30 min at 40 °C to fully dissolve gelatin crystals while avoiding gelatin degradation. After this period, 4 mL of 25% NH_4OH solution was added, and the stirring was continued for 1 min to homogenize the mixture. The obtained solution was transferred to a Petri dish with a diameter of 150 mm to form a flat, homogeneous layer. The dish with the solution was then capped and refrigerated at 7 °C for 1 h to cross-link the gel. The dish with formed gel was subsequently moved to a flat surface at ambient temperature, and the aqueous solution containing zinc ions was slowly poured over the surface of the gel. After 24 h of precipitation at ambient temperature, a dense rough layer of white solid was obtained at the gel/liquid interface. The solution on the top was decanted, and the white solid layer was then mechanically peeled off from the surface of the gel and broken into pieces using the stream of distilled water. The aqueous suspension containing the precipitate was washed with distilled water and centrifuged at ~7370 g for 5 min three times to remove residual impurities. The obtained slurry was oven-dried at 75 °C for 24 h under atmospheric pressure. The dry precipitate was subsequently calcinated at 400 °C for 1 h under atmospheric pressure to improve the crystallinity of ZnO and partially decompose the gelatin.

GM ZnO NPs synthesized at the surface of hydrogels with 5 wt%, 10 wt%, and 15 wt% of gelatin content will be designated in the further text as ZnO-5, ZnO-10, and ZnO-15, respectively.

2.3. Characterization of GM ZnO NPs

Characterization of synthesized GM ZnO NPs was performed by X-ray powder diffraction (XRD), scanning electron microscopy (SEM), Fourier-transform infrared spectroscopy-attenuated total reflectance (FTIR-ATR), thermal analyses (differential thermal analysis (DTA) and thermogravimetry (TG)), photon correlation spectroscopy (PCS), zeta potential measurements, and inductively coupled plasma-mass spectrometry (ICP-MS).

XRD data were collected using a Philips PW-1050 diffractometer, operated at 40 kV/20 A with Cu $K_{\alpha 1,2}$ radiation. The diffraction peaks were recorded over a 2θ range of 10-70 ° with a step of 0.05 ° and a counting time of 5 s per step. The observed crystal phases were acknowledged by comparing the recorded data with the one reported in the Joint Committee of Powder Diffraction Standards (JCPDS) database.

The microstructure of the GM ZnO nanopowders with thin gold coating was imaged using the field emission scanning electron microscope FE-SEM, TESCAN MIRA 3 XMU, operated at 20 keV.

FTIR-ATR spectra of the powders were recorded using the Thermo Scientific Nicolet iS10 FTIR Spectrometer instrument equipped with Smart iTX ATR Diamond accessory. The spectra were acquired over the spectral range of 400-4000 cm^{-1} with the resolution of 0.5 cm^{-1} and subsequently normalized to the highest absorption band intensity.

The thermal stability of the air-dried powders was investigated using the simultaneous TG/DTA analysis with the instrument Setsys, SETARAM Instrumentation, Caluire, France in the temperature range from 40 °C up to 800 °C in the air atmosphere under the flow rate of 20 mL min^{-1}. The sample powder was initially stabilized at 40 °C for 5 min and then heated to 800 °C with a controlled heating rate of 10 °C min^{-1}. All TG and DTA curves were normalized per sample mass.

The average particle size (Z_{avg}) and polydispersity index (PDI) in the tested samples were determined by PCS using a ZetasizerNano ZS90 (Malvern Instruments, Worcestershire, United Kingdom) equipped with He-Ne laser light of 633 nm wavelength. Aqueous suspensions (100 μg mL^{-1}) of ZnO-5, ZnO-10, and ZnO-15 powders were prepared in deionized water using a Sonorex RK 102 H ultrasonic bath (Bandelin, Germany). The detection of scattered light was performed at an angle of 90 °. All measurements were

performed consecutively in triplicate at a temperature of 25 ± 0.1 °C. Recorded measurement data were analyzed with Dispersion Technology Software, and the obtained results are reported in the form mean value ± standard deviation.

The zeta potential (ζ) of ZnO-5, ZnO-10, and ZnO-15 powders was measured using a ZetasizerNano ZS90 (Malvern Instruments, Worcestershire, United Kingdom). Before the measurements, the operating conditions were confirmed and adjusted using a calibrated latex dispersion supplied by the instrument manufacturer. Aqueous suspensions (100 μg mL^{-1}) of the tested materials were prepared in deionized water using a Sonorex RK 102 H ultrasonic bath (Bandelin, Germany) and transferred to a disposable folded capillary DTS1070. Each measurement was carried out in triplicate at 25 ± 0.1 °C. The results of zeta potential measurements are presented as mean value ± standard deviation.

The solubility of GM ZnO NPs was determined by measuring the content of zinc ions in the solution. Quantification of zinc was carried out using the ICP-MS instrument (ICP-MS, iCAP Qc, Thermo Scientific, United Kingdom). Suspensions of ZnO-5, ZnO-10, and ZnO-15 powders (100 μg mL^{-1}) were prepared in physiological saline solution (0.9% NaCl) and sustained for 24 h at 37 ± 1 °C (Vaciotem, JP Selecta, Spain) before the measurements.

2.4. Cell culture

Human hepatocellular carcinoma cells (HepG2) were obtained from the European Collection of Authenticated Cell Cultures (Salisbury, UK; Cat. N° 85011430). The cells were grown at 37 °C and 5% CO_2 in Eagle Minimal Essential Medium supplemented with 10% FBS, 2 mmol L^{-1} L-glutamine, 1% non-essential amino acids, and 100 IU mL^{-1} penicillin/streptomycin. Cells were routinely checked for mycoplasma (MycoAlert™, Lonza, Walkersville, USA). The experiments were performed on HepG2 cells between cell passages 15 and 20.

2.5. Determination of cytotoxicity (MTS assay)

HepG2 cells were seeded at a density of 8000 cells per well (40000 cells mL^{-1}) into 96-well plates (Nunc, Naperville IL, USA) for 24 h at 37 °C and 5% CO_2. The viability of HepG2 cells after 24 h of exposure to

GM ZnO NPs (ZnO-5, ZnO-10, and ZnO-15) at graded concentrations (0.01, 0.1, 1, 10, and 100 μg mL^{-1}) was tested with the MTS assay. MTS and PMS solutions were mixed in the ratio 20:1. The final solution was added 1:5 to treated cells that were incubated for additional 3 h. Subsequently, the biological reduction of the tetrazolium to the formazan by viable cells was analyzed by measuring the absorbance of the control and exposed cells at the wavelength of 490 nm using a spectrofluorimeter (Synergy™ Mx, BioTek Instruments). Experiments were performed in five replicates. Etoposide (ET; 125 μg mL^{-1}) was used as a positive control. Statistical significance between treated groups and the solvent control was determined by one-way analysis of variance (ANOVA), with Dunnett's Multiple Comparison test; $P < 0.05$ was considered as statistically significant.

2.6. Determination of intracellular ROS formation (DCFH-DA assay)

The formation of intracellular ROS was measured using a fluorescent probe, DCFH-DA as described by Osseni et al. (1999) with minor modifications (Petković et al. (2011)). Briefly, HepG2 cells were seeded at a density of 15000 cells per well (75000 cells mL^{-1}) into black 96-well plates (Nunc, Naperville IL, USA) for 24 h at 37 °C and 5% CO_2. After the incubation, the cells were exposed to DCFH-DA (20 μmol L^{-1}) in PBS for 30 min. Subsequently, DCFH-DA was removed, and cells were treated with GM ZnO NPs (ZnO-5, ZnO-10, and ZnO-15) at graded concentrations of 0, 0.1, 1, 10, and 100 μg mL^{-1} in PBS. The negative control (non-treated cells), solvent control (1% ethanol), and positive control (TBHP; 0.5 mmol L^{-1}) were included in each experiment. For kinetic analyses, the plates were maintained at 37 °C, and the fluorescence intensity was determined every 30 min using a microplate reading spectrofluorimeter (Synergy™ Mx, BioTek Instruments) at the excitation and emission wavelengths of 485 and 530 nm, respectively. Each experiment was performed in five replicates.

The statistical significance between control (solvent) and exposed groups was determined using Kruskal–Wallis one-way ANOVA with Dunnett's Multiple Comparison test; $P < 0.05$ was considered as statistically significant.

2.7. Determination of genotoxicity (alkaline comet assay)

The formation of DNA strand breaks in HepG2 cells due to the exposure to GM ZnO NPs (ZnO-5, ZnO-10, and ZnO-15) at concentrations of 0, 0.1, 1, 10, and 100 μg mL^{-1} was analyzed with the alkaline comet assay according to Singh et al. (1988) with details described in Møller et al. (2020). After 24 h of exposure, the cells were washed with PBS, trypsinized, and centrifuged. 30 μl of cell suspension was mixed with 1% LMP agarose, added to fully frosted slides precoated with 1% NMP agarose, and lysed (2.5 M NaCl, 100 mmol L^{-1} EDTA-Na_2, 10 mmol L^{-1} Tris, 1% Triton X-100; pH 10; 1 h at 4 °C). After the lysis, the slides were placed in electrophoresis buffer (1 mmol L^{-1} M EDTA-Na_2, 300 mmol L^{-1} NaOH; pH 13; 20 min at 4 °C) for DNA unwinding, and electrophoresis was conducted at 1 V cm^{-1} (20 min at 4 °C). Finally, the slides were neutralized (0.4 M Tris buffer; pH 7.5; 15 min at 4 °C). For DNA damage analysis, the gels were stained with GelRed Nucleic Acid Stain (1:3333), and the images observed using the fluorescence microscope (Eclipse 800, Nikon) and image analysis software Comet IV (Perceptive Instruments, Bury St Edmunds, UK). Fifty randomly selected nuclei were analyzed per experimental point, and the DNA damage was expressed as the percentage of DNA in the comet tail. The experiments were repeated three times independently. Benzo(a)pyrene (BaP; 30 μmol L^{-1}) was used as a positive control. One-way ANOVA was used to analyze the differences in the percentage of tail DNA between solvent control and exposed cells. For comparing the exposed groups to the control group Dunnett's Multiple Comparison test was used; $P < 0.01$ was considered as statistically significant.

3. Results

3.1. Thermal analysis (TG/DTA) of GM ZnO NPs

TG and DTA curves (**Fig. 1**) were recorded starting from the GM ZnO NP powders before calcination to estimate their thermal stability. According to the DTA curves, two processes occur during the heating, which correspond to water loss and gelatin degradation. Loss of adsorbed and bound water occurs from 40 °C up to about 240 °C, which is also reflected in the 13% of weight loss appearing in the TG curves. Gelatin degradation starts at 240 °C and reaches its peak on average at around 343 °C. As shown by DTA curves, the entire process of gelatin degradation occurs through three stages comprising various degrees of decomposition, oxidation, and gasification [25, 80]. These stages are related to the approximate temperature

ranges from 240 °C to 400 °C, 400 °C to 490 °C, and from 490 °C to 800 °C. The first stage corresponds to the mass loss of 18%, the second stage to the mass loss of 3%, and the final stage to the mass loss smaller than 1%.

According to DTA curves, gelatin degradation peak position shifts towards higher temperatures with a decrease in the gelatin content of the hydrogel during the synthesis of NPs. This shift is more than 10 °C for ZnO-5 compared to the peak positions for ZnO-10 and ZnO-15. Similar trends can be observed for temperatures at the onsets of other characteristic processes or their stages. Improvement in the thermal stability of GM ZnO NPs can be explained by the stronger interaction of the ZnO surface and adsorbed gelatin during the synthesis at the hydrogel surface with lower gelatin content.

3.2. XRD characterization of GM ZnO NPs

Recorded diffractograms of the synthesized GM ZnO NPs (**Fig. 2**) confirmed that the only crystalline phase present in the prepared samples is the one originating from the ZnO hexagonal wurtzite structure crystallized on the surface of the gelatin matrix. All reflections appear to be in good agreement with JCPDS-no. 89-7102 [81].

Diffraction patterns originating from impurities were not detected, which indicates a pure hexagonal ZnO phase. The occurrence of the broad diffraction peaks with high intensity verifies the crystalline nature of ZnO NPs. All prepared samples have overall similar XRD patterns with some differences in crystallite size and relative peak intensity level. After fitting the diffraction peaks corresponding to the crystallographic directions [100], [002], and [101] the mean crystallite size was estimated to be below 12.1 nm in all samples (for fitting and calculation details refer to **Online Resource 1**). The average crystallite size of ZnO-5 powder was found to be slightly larger than for ZnO-10 and ZnO-15 powders. Intensity level deviations are caused by the random orientation of crystallographic planes. As evidenced by XRD measurements, gelatin modification did not induce changes in the crystal structure of ZnO NPs.

3.3. SEM characterization of GM ZnO NPs

The overall morphology of the prepared GM ZnO NPs is similar in all samples (**Fig. 3**). SEM images show the sheet-shaped GM ZnO NPs with irregular edges stacked into flake-like structures and larger aggregates of submicron size. Almost no difference can be observed in the microstructure of ZnO-10 and ZnO-15 powders. ZnO-5 powder exhibits a slightly larger particle size and softer agglomerates.

3.4. FTIR-ATR characterization of GM ZnO NPs

We recorded the FTIR-ATR spectrum of the pure air-dried gelatin film (with initial gelatin content of 10 wt%) and the FTIR-ATR spectra of GM ZnO NPs after calcination (**Fig. 4**). Gelatin film exhibited multiple bands characteristic of peptides or proteins. Inter-atomic vibration bands in the fingerprint region (below 1000 cm^{-1}) are characteristic for metal oxides [82]. Such distinct bands were detected in our ZnO NPs together with the absorption bands corresponding to residual acetate impurities and organic residues after gelatin decomposition and oxidation.

Fig. 4a shows the FTIR-ATR spectrum of pure air-dried gelatin film. Gelatin absorption bands at 3322, 3089, 1652, and 1558 cm^{-1} can be attributed to amide A, amide B, amide I, and amide II, respectively [83]. The absorption band at 3322 cm^{-1} overlaps with the broad H-O-H stretching band of adsorbed water. C-H stretching is indicated by the bands at 2964 and 2882 cm^{-1}, while the band at 1456 cm^{-1} can be attributed to C-H bending. Absorption bands at 1404, 1339, 1244, and 1204 cm^{-1} correspond to the amide III region. Bands at 1244 and 1404 cm^{-1} in this region are overlapped with the C-O stretching bands of carboxyl groups. The remaining absorption bands at 1083 cm^{-1} and 668 cm^{-1} were attributed to the C-O stretching of carbohydrate residues [84] and out-of-plane N-H bending (amide V band [83]), respectively.

Fig. 4b illustrates the FTIR-ATR spectra of GM ZnO NPs synthesized using hydrogels with different gelatin content (ZnO-5, ZnO-10, and ZnO-15). The absorption band at 3363 cm^{-1} corresponds to the O-H stretching of adsorbed water, while the bands at 2960, 2927, and 2856 cm^{-1} are C-H stretching modes. Bands at 1652 and 1552 cm^{-1} are amide I and amide II, while the bands at 1506 and 1354 cm^{-1} can be attributed to asymmetric and symmetric N-O stretching [85], respectively. Absorption bands at 1393, 1245, and 1044 cm^{-1} appear due to the C-O stretching, while the bands at 1428 and 942 cm^{-1} indicate O-H bending of carboxyl groups. The bands at 830 and 738 cm^{-1} were assigned to the =C-H and C-H out of plane bending,

respectively. The remaining absorption bands correspond to the Zn-O stretching lattice vibrations for the octahedral (692 cm^{-1}) and tetrahedral (514 and 472 cm^{-1}) coordination.

3.5. Determination of particle size, zeta potential, and solubility of GM ZnO NPs

Obtained results of particle size measurements by PCS reveal high values of PDI and the formation of submicron-sized agglomerates in aqueous suspension for all GM ZnO NP powders. All mean values of zeta potential are lower than 20 mV indicating the limited stability of GM ZnO NPs in aqueous suspension. Results of particle size and zeta potential measurements are listed in **Table 1**.

Table 1. Average particle size (Z_{avg}), polydispersity index (PDI), and zeta potential (ζ) of GM ZnO NP powders suspended in deionized water at 25 ± 0.1 °C reported with the corresponding standard deviation.

Sample powder	Z_{avg} (nm)	PDI	ζ (mV)
ZnO-5	447.3 ± 19.5	1	18.0 ± 1.4
ZnO-10	449.9 ± 37.5	0.738 ± 0.157	18.5 ± 1.5
ZnO-15	325.4 ± 56.1	0.744 ± 0.228	15.7 ± 1.2

The quantity of zinc formed by the dissolution of GM ZnO NPs in physiological saline solution after 24 h of incubation at 37 ± 1 °C was similar for all powders and can be represented in the form of cumulative mean ± standard deviation as 9.58 ± 2.93 μg mL^{-1}.

3.6. Biocompatibility studies

3.6.1. *In vitro* cytotoxicity of GM ZnO NPs

The cytotoxic activity of GM ZnO NPs (0, 0.01, 0.1, 1, 10, and 100 μg mL^{-1}) was determined with the MTS assay after 24 h of exposure in HepG2 cells (**Fig. 5**). The viability of HepG2 cells exposed to ZnO-10 and ZnO-15 was significantly decreased only at the highest tested concentration (100 μg mL^{-1}) on average to 80 and 87%, respectively, compared to control, while ZnO-5 did not influence cell viability. The viability of cells in the solvent control did not differ significantly from that of non-treated control cells (data not shown).

Based on these results, the concentrations that did not decrease cell viability for more than 25% were used in further experiments for the determination of ROS formation and DNA damage induction.

3.6.2. Induction of intracellular ROS by GM ZnO NPs

The induction of intracellular ROS formation by GM ZnO NPs was determined by the fluorescent probe DCFH-DA. The probe is hydrolyzed by intracellular esterases to a non-fluorescent product DCFH, which in the presence of ROS rapidly oxidizes to the highly fluorescent 2',7'-dichlorofluorescein (DCF). The DCF fluorescence intensity is proportional to the amount of ROS formed intracellularly. The results showed that none of the studied GM ZnO NPs increased the formation of ROS during a 2.5 h period (**Fig. 6**). The positive control (0.5 mmol L^{-1} TBHP) induced about an 8-fold increase in DCF fluorescence over the control cells after 2.5 h of exposure, confirming the expected performance of the test system.

3.6.3. Induction of DNA strand breaks

HepG2 cells were exposed to graded doses (0.1, 1, 10, and 100 μg mL^{-1}) of GM ZnO NPs for 24 h and the induction of DNA strand breaks detected by the comet assay was compared to evaluate the genotoxic potential of GM ZnO NPs. All GM ZnO NPs induced DNA damage only at the highest tested concentration of 100 μg mL^{-1} (**Fig. 7**).

4. Discussion

4.1. Proposed mechanism of GM ZnO NPs formation

The formation of the GM ZnO NPs is primarily driven by the diffusion of ammonia through the porous gelatin hydrogel matrix. The matrix exhibits complex porosity patterns that strongly depend on gelatin content in the hydrogel [86]. Zinc aquo complexes undergo deprotonation in the presence of excess hydroxyl ions produced by the hydrolysis of ammonia diffusing towards the interfacial region. This process enables the nucleation and growth of templated ZnO nanocrystals. Formation of ZnO NPs involving $Zn(CH_3COO)_2$ and NH_4OH as precursors is a complex process that can be described by the set of chemical reactions revealing different pathways for ZnO precipitation [87].

Surface pores of the gelatin hydrogel play a crucial role in controlling the nucleation and subsequent self-organization of precipitated ZnO nanocrystals. Hydrogel pores facing the aqueous $Zn(CH_3COO)_2$ solution above can serve as a template and stabilizer of nanocrystals, while abundant polar groups of gelatin molecules (-COOH and $-NH_2$) can act as coordination sites [25].

The initial electrostatic interaction between the zinc aquo complex and polar groups of gelatin facilitates the adsorption of gelatin onto the surface of ZnO. Diffusion of ammonia towards the gel/liquid interface weakens the cross-linking ability of gelatin at the surface presumably due to the localized pH increase, and thus further aids the detachment of gelatin macromolecules from the hydrogel structure. After nucleation at the provided coordination sites, the growth of ZnO crystals is mainly directed perpendicularly to the c-axis because of gelatin adsorption on polar surfaces as reported in previous studies [24, 25], which results in the initial nanosheet particle morphology. Further assembly of nanosheets into aggregates is dictated by their size and the structure of porosity at the gelatin hydrogel surface.

4.2. Synthesis parameters and physicochemical characterization of GM ZnO NPs

We propose the simple and cost-effective synthesis of GM ZnO NPs as a means to design safer nanomaterial with low toxicity. NPs precipitate at the interface of $Zn(CH_3COO)_2$ solution and gelatin hydrogel containing NH_4OH. The diffusion of a precursor through the porous hydrogel matrix towards the gel/liquid interface controls precipitation synthesis. Gelatin content in the hydrogel indirectly affects particle size and aggregation, as it defines the porosity patterns and mean pore size of the hydrogels. Nindiyasari et al. (2014) qualitatively studied the porosity of the gelatin hydrogel structure. They observed that pore walls become thicker, while the overall pore size becomes reduced with the increase in gelatin content. According to their findings, pore sizes in hydrogels with gelatin content of 5 wt% or higher are expected to be in the μm range. The estimated size of the pores is sufficiently large for the efficient diffusion of ammonia as well as the aggregation of NPs through self-assembly.

Gelatin content in the hydrogel also determines the degree of physical cross-linking and the surface density of coordination sites templating ZnO precipitation. Hydrogels with higher gelatin content have more densely packed coordination sites and stronger cross-linking. Hence, an increase in gelatin content leads to a greater

number of NPs which can be formed at the surface while the adsorption interactions of gelatin macromolecules with ZnO become weaker. TG/DTA analysis in our study revealed that GM ZnO NPs grown on the surface of hydrogels with the lowest gelatin content have the best thermal stability, which indicates the strongest adsorption interactions between gelatin and ZnO in this case. Differences in the thermal stability of the GM ZnO NPs are also reflected in the FTIR-ATR spectra of NP powders calcinated under the same conditions.

TG/DTA analysis additionally provides an important insight into the optimal calcination temperature which can result in partial decomposition and removal of gelatin, while ensuring that only the small amount of strongly bound organic residues acts as NP modifier.

FTIR-ATR spectra of calcinated powders indicate the presence of ZnO and organic residues containing mainly short carbon backbones with some amount of oxidized nitrogen functionalities. With the increase of gelatin content in the hydrogel, a gradual change can be observed in the intensity of several absorption bands corresponding to organic residues after calcination. These changes in the spectra can be attributed to the different extents of gelatin degradation at the NP surface after thermal treatment.

Results of particle size measurements using PCS reflect the strongly polydisperse nature and very broad size distribution of GM ZnO NPs in aqueous suspension with average PDI values above 0.7. The obtained PDI values are comparable with PDI values of ZnO NPs obtained by some green synthesis methods [88, 89]. GM ZnO NPs exhibit a positive surface charge indicated by the mean zeta potential values in the approximate range from 15 mV to 19 mV. This range of zeta potential values indicates incipient instability and a tendency to form aggregates [90], which is in accordance with the results of particle size measurements by PCS. Uncoated synthesized ZnO NPs with wurtzite crystal structure typically exhibit positive surface charge and zeta potential values that can reach around 25 mV after coating at neutral pH [91]. Therefore, modification of ZnO NPs with gelatin residues did not significantly alter their colloidal stability in aqueous suspension.

We measured the solubility of GM ZnO NPs in physiological saline solution (0.9% or 154 mM NaCl) after 24 h at 37 °C. The physiological saline solution was our medium of choice because its osmolarity

corresponds with the osmolarity of the extracellular liquid and its constituents (Na^+ and Cl^- ions) dominate in the extracellular liquid. Measured solubility of GM ZnO NPs is comparable with the solubility of unmodified ZnO NPs in relevant media for biological applications such as Dulbecco's Modified Eagle's Medium and nanopure water under similar experimental conditions [92]. Hence, the presence of gelatin residues also does not seem to significantly affect the solubility of GM ZnO NPs.

Research on nanoparticle-protein interactions shows that protein corona can significantly affect the behavior and toxicity of NPs [93, 94]. Hence, initial gelatin interactions with ZnO NPs require more detailed investigation which is beyond the scope of this study. As gelatin represents the mixture of peptides and proteins [95] such interactions are difficult to analyze and should be a topic for further research.

Relevant comparisons can be made between our method for the synthesis of ZnO NPs and standard co-precipitation synthesis methods or predominant green synthesis methods based on biological extracts of plants and algae. Co-precipitation methods are typically performed in bulk solution at elevated temperature, and they produce agglomerated NPs with limited biocompatibility due to the use of harsh chemicals as precursors in large amounts [7, 8]. Phytochemical synthesis methods are eco-friendly and the obtained ZnO NPs commonly exhibit good biocompatibility. However, there are also some disadvantages imposing limitations on the wider use of phytochemical methods. These methods require long preprocessing times to isolate and characterize the biological extract, biological extract usually has a limited lifetime and complex chemical composition, exact synthesis mechanisms are still not elucidated, and resulting ZnO NPs exhibit a broad size distribution [8, 96].

Our synthesis method exploits the possibility of chemical precipitation at the interface between the gelatin hydrogel and aqueous electrolyte enabling the simultaneous synthesis of ZnO NPs and their modification with gelatin components. After a short thermal processing step, we obtain GM ZnO NPs that are highly biocompatible and exhibit low toxicity. The method relies on well-known precipitation mechanisms and the use of commercially available standardized gelatin, which opens the possibility to easily scale up the fabrication. While our synthesis approach does not offer significant improvements in terms of size

distribution and particle aggregation, it is simple, cost-effective, and successfully combines the useful features of precipitation and phytochemical methods.

The approach of ZnO NP precoating using supplemented cell culture medium [71] can be used to achieve the low toxicity levels of resulting ZnO NPs that are comparable to our approach in terms of cell viability and ROS generation. However, the use of supplemented cell culture medium significantly increases the cost, complexity, and duration of the fabrication process required to obtain modified ZnO NPs with low toxicity. Our approach enables the use of low-cost and readily available gelatin while incorporating the required ZnO NP modification already in the initial synthesis stage thus eliminating the need for the additional modification step.

The synthesis approach presented in this study is not necessarily limited to the fabrication of GM ZnO NPs. Its use should be further evaluated for the gelatin modification of other NPs that can be synthesized via precipitation under similar experimental conditions.

4.3. Toxicity evaluation of GM ZnO NPs

We investigated the cytotoxic and genotoxic effects of three types of GM ZnO NPs (ZnO-5, ZnO-10, and ZnO-15) in the human hepatocellular carcinoma (HepG2) cell line. This cell line was selected for studying the toxic activities of ZnO NPs because it is widely used in toxicological studies as one of the test systems of choice. The HepG2 cells express wild-type tumor suppressor TP53 [97], which makes them a suitable model for studying p53 regulated response to DNA damage, have a known karyotype [98] and have retained the activity of several phase I and II metabolic enzymes involved in the metabolism and detoxification of xenobiotics substances [99]. *In vitro* toxicity studies with ZnO NPs have demonstrated that their toxic effects are mainly related to the generation of ROS with the induction of oxidative stress [100, 101], which consequently induces damage to cellular macromolecules, including DNA [100–104], while at higher concentrations exposure to ZnO NPs is associated with apoptotic death [100]. It was previously reported that ZnO NPs after 24 h of exposure decreased the viability of HepG2 cells at doses $\geq$ 10 μg mL^{-1} [105] and $\geq$ 14 μg mL^{-1} [100], human peripheral blood lymphocytes at doses $\geq$ 1 mmol L^{-1} ($\approx$ 80 μg mL^{-1}) [101], nasal mucosa cells at doses $\geq$ 5 μg mL^{-1} [103], human lung epithelial cells (L-132) at doses $\geq$ 25 μg mL^{-1} [106],

human monocytes (THP-1) at ≥ 10 μg mL^{-1} [106], and human colon carcinoma cells (Caco-2) [107]. Divya et al. (2018) synthesized gelatin-coated ZnO NPs for biomedical applications using a co-precipitation method involving thermal treatment. The synthesized gelatin-coated ZnO NPs significantly reduced the viability of HepG2 cells at doses ≥ 25 μg mL^{-1}, while at the dose of 100 μg mL^{-1}, viability was reduced by nearly 90% compared to the control. The GM ZnO NPs synthesized in this study, namely ZnO-10 and ZnO-15 slightly reduced cell viability at 100 μg mL^{-1}, but the decrease was less than 20% compared to control. ZnO-5 did not affect cell survival under applied exposure conditions.

The induction of ROS was measured in HepG2 cells after a short time of exposure up to 150 min using a DCFH-DA fluorescent probe. The results showed that GM ZnO NPs at applied conditions did not induce ROS formation. On the contrary, ZnO NP-induced oxidative stress has been demonstrated in HepG2 cells exposed to 20 μg mL^{-1} [100] and in mouse podocytes [108] exposed to 10, 50, and 100 μg mL^{-1} of ZnO NPs for 6 h. ZnO NP-induced ROS formation has also been reported in other cell lines. In the human embryonic kidney (HEK-293) ZnO-NPs induced ROS formation was observed at concentrations > 25 μg mL^{-1} after 48 h of incubation [109]. ZnO-NP induced ROS formation detected by DCF probe was demonstrated also in RAW 264.7 with an immediate strong increase in fluorescence whereas no increase of DCF fluorescence was observed in BAES-B cells [110].

The comet assay was applied to assess DNA damage in HepG2 cells after exposure to GM ZnO NPs. Genotoxic effects induced by GM ZnO NPs have been observed only at very high concentrations of 100 μg mL^{-1} that are not relevant for human exposure. Genotoxic effects of ZnO NPs were detected in many of the previously published studies. The formation of DNA strand breaks by ZnO NPs has been reported at concentrations that were lower from those used in the present study: in HepG2 cell (14 μg mL^{-1}; 6 h) [100], in human peripheral blood lymphocytes (≥ 40 μg mL^{-1}; 24 h) [101], human nasal mucosa cells (≥ 0.1 μg mL^{-1}; 24 h) [103], human colon carcinoma (Caco-2) cells (6.4 μg mL^{-1}; 24 h) [107], human alveolar epithelial (A549) (0.1 and 3 μg mL^{-1}; 3 and 24 h, respectively) and lymphoblastoid TK6 cells (0.42 μg mL^{-1}; 3 h) [104]. Most of these studies demonstrated that DNA damage is ROS mediated [100, 101, 104, 107]. The low genotoxic potential of GM ZnO NPs can be ascribed to the lack of their ability to induce ROS formation.

The toxicity of ZnO NPs draws the attention of biomedical researchers as it presents a major issue preventing the wider use of these promising materials. Functionalization of ZnO NPs is one of the proposed approaches for toxicity reduction that can enhance NP selectivity while retaining the intended NP activity [2]. However, the effectiveness of the specific functionalization approach must be experimentally verified as the activity of ZnO NPs can result from complex mechanisms.

For example, the antibacterial activity of ZnO NPs may rely on similar mechanisms as the ones responsible for toxicity in HepG2 cells. Hence, there is a possibility that reduced toxicity of GM ZnO NPs can be correlated with diminished antibacterial activity. Even in such a case, GM ZnO NPs that exhibit a lack of antibacterial activity and low toxicity levels can be good candidates for the dietary supplementation of zinc. GM ZnO NPs with weak antibacterial properties may enable the preservation of the microbiota within the gastrointestinal tract, which is an important requirement for NP-based dietary supplements [87].

Our findings suggest that the reduction in toxicity of ZnO NPs is correlated with the strength of adsorption interactions between the gelatin hydrogel and ZnO NP surface. Hence, the potency of GM ZnO NPs may be adjusted via the changes in hydrogel gelatin content to find the optimal balance between the toxicity and selective activity of modified ZnO NPs.

5. Conclusions

We proposed the concept of using biocompatible organic residues produced by gelatin decomposition for surface modification of ZnO NPs to reduce their toxicity in biomedical applications. Our goal in this study was to fabricate modified ZnO NPs that are safe by design.

An innovative, simple, and cost-effective method for the precipitation synthesis of GM ZnO NPs at the interface of gelatin hydrogel and an aqueous electrolyte was described. The properties of obtained NPs can be modulated by the changes in hydrogel properties which are mainly directly determined by gelatin content. GM ZnO NPs fabricated using the proposed method did not induce ROS formation at doses relevant for human exposure and exhibited no cytotoxic nor significant genotoxic activity towards HepG2 cells. Adsorption interactions between the gelatin hydrogel and ZnO nanocrystals together with the appropriate

thermal treatment conditions for the partial decomposition of gelatin at the NP surface proved to be crucial factors in achieving reduced toxicity.

Our future research will be focused on investigating the antibacterial activity of fabricated GM ZnO NPs to assess their potential for biomedical applications and dietary supplementation.

Electronic supplementary material

Online Resource 1: Crystallite size estimation for gelatin modified zinc oxide nanoparticles

Declarations

Funding

Funds for the realization of the research work in the Institute of Technical Sciences of SASA are provided by the Ministry of Education, Science and Technological Development of the Republic of Serbia according to the Agreement on realization and financing of scientific research work of the Institute of Technical Sciences of SASA in 2020 (Record number: 451-03-68 / 2020-14 / 200175). This work was also supported by a COST Action CA15114, a bilateral collaboration between Serbia and Slovenia (BI-RS/16-17-039) and Slovenian Research Agency: Program P1-0245. The funding sources were not involved in the research process and the decisions related to publishing.

Conflicts of interest/Competing interests

The authors have no relevant financial or non-financial interests to disclose.

Ethics approval

Not applicable

Consent to participate

Not applicable

Consent for publication

Not applicable

Availability of data and material

The data and materials that support the findings of this study are available from the corresponding author upon reasonable request.

Code availability

Codes for calculations are available from the corresponding author upon reasonable request.

Authors' contributions

Conceptualization: Željko Janićijević; **Data curation**: Željko Janićijević, Ana Stanković, Bojana Žegura, . Đorđe Veljović; **Formal analysis:** Željko Janićijević, Ana Stanković, Bojana Žegura; **Funding acquisition:** Metka Filipič, Magdalena Stevanović; **Investigation:** Željko Janićijević, Ana Stanković, Bojana Žegura, Đorđe Veljović, Magdalena Stevanović, Ljiljana Djekić, Danina Krajišnik; **Methodology:** Željko Janićijević, Ana Stanković, Bojana Žegura, Magdalena Stevanović, Ljiljana Djekić, Danina Krajišnik; **Project administration:** Metka Filipič, Magdalena Stevanović; **Resources:** Metka Filipič, Magdalena Stevanović; **Software:** Željko Janićijević; **Supervision:** Metka Filipič, Magdalena Stevanović; **Validation:** Željko Janićijević, Ana Stanković, Bojana Žegura, Đorđe Veljović; **Visualization:** Željko Janićijević, Ana Stanković, Bojana Žegura; **Writing – original draft:** Željko Janićijević, Ana Stanković, Bojana Žegura; **Writing – review & editing:** Željko Janićijević, Ana Stanković, Bojana Žegura, Đorđe Veljović, Ljiljana Djekić, Danina Krajišnik, Metka Filipič, Magdalena Stevanović

References

1. Kumar P, Kumar P, Deep A, Bharadwaj LM (2013) Synthesis and conjugation of ZnO nanoparticles with bovine serum albumin for biological applications. Appl Nanosci 3:141–144. https://doi.org/10.1007/s13204-012-0101-0

2. Mishra PK, Mishra H, Ekielski A, et al (2017) Zinc oxide nanoparticles: a promising nanomaterial for biomedical applications. Drug Discov Today 22:1825–1834. https://doi.org/10.1016/j.drudis.2017.08.006

3. Jiang J, Pi J, Cai J (2018) The Advancing of Zinc Oxide Nanoparticles for Biomedical Applications.

Bioinorg Chem Appl 2018:1–18. https://doi.org/10.1155/2018/1062562

4. Fakhroueian Z, Katouzian F, Esmaeilzadeh P, et al (2019) Enhanced engineered ZnO nanostructures and their antibacterial activity against urinary, gastrointestinal, respiratory and dermal genital infections. Appl Nanosci 9:1759–1773. https://doi.org/10.1007/s13204-019-00996-5

5. Abedini M, Shariatmadari F, Torshizi MAK, Ahmadi H (2017) Effects of a dietary supplementation with zinc oxide nanoparticles, compared to zinc oxide and zinc methionine, on performance, egg quality, and zinc status of laying hens. Livest Sci 203:30–36. https://doi.org/10.1016/j.livsci.2017.06.010

6. Pei X, Xiao Z, Liu L, et al (2019) Effects of dietary zinc oxide nanoparticles supplementation on growth performance, zinc status, intestinal morphology, microflora population, and immune response in weaned pigs. J Sci Food Agric 99:1366–1374. https://doi.org/10.1002/jsfa.9312

7. Kolodziejczak-Radzimska A, Jesionowski T (2014) Zinc oxide-from synthesis to application: A review. Materials (Basel) 7:2833–2881. https://doi.org/10.3390/ma7042833

8. Chan YY, Pang YL, Lim S, Chong WC (2021) Facile green synthesis of ZnO nanoparticles using natural-based materials: Properties, mechanism, surface modification and application. J Environ Chem Eng 9:105417. https://doi.org/10.1016/j.jece.2021.105417

9. Stanković A, Dimitrijević S, Uskoković D (2013) Influence of size scale and morphology on antibacterial properties of ZnO powders hydrothemally synthesized using different surface stabilizing agents. Colloids Surfaces B Biointerfaces 102:21–28. https://doi.org/10.1016/j.colsurfb.2012.07.033

10. Stanković A, Sezen M, Milenković M, et al (2016) PLGA/Nano-ZnO Composite Particles for Use in Biomedical Applications: Preparation, Characterization, and Antimicrobial Activity. J Nanomater 2016:1–10. https://doi.org/10.1155/2016/9425289

11. Wahab R, Kim Y-S, Shin H-S (2009) Synthesis, Characterization and Effect of pH Variation on Zinc Oxide Nanostructures. Mater Trans 50:2092–2097. https://doi.org/10.2320/matertrans.M2009099

12. Talam S, Karumuri SR, Gunnam N (2012) Synthesis, Characterization, and Spectroscopic Properties of ZnO Nanoparticles. ISRN Nanotechnol 2012:1–6. https://doi.org/10.5402/2012/372505

13. Venu Gopal VR, Kamila S (2017) Effect of temperature on the morphology of ZnO nanoparticles: a comparative study. Appl Nanosci 7:75–82. https://doi.org/10.1007/s13204-017-0553-3

14. Nandhini G, Suriyaprabha R, Maria Sheela Pauline W, et al (2018) Influence of solvents on the changes in structure, purity, and in vitro characteristics of green-synthesized ZnO nanoparticles from Costus igneus. Appl Nanosci 8:1353–1360. https://doi.org/10.1007/s13204-018-0810-0

15. Bagabas A, Alshammari A, Aboud MF, Kosslick H (2013) Room-temperature synthesis of zinc oxide nanoparticles in different media and their application in cyanide photodegradation. Nanoscale Res Lett 8:516. https://doi.org/10.1186/1556-276X-8-516

16. Mohan Kumar K, Mandal BK, Appala Naidu E, et al (2013) Synthesis and characterisation of flower shaped zinc oxide nanostructures and its antimicrobial activity. Spectrochim Acta - Part A Mol Biomol Spectrosc 104:171–174. https://doi.org/10.1016/j.saa.2012.11.025

17. Kumar SS, Venkateswarlu P, Rao VR, Rao GN (2013) Synthesis, characterization and optical properties of zinc oxide nanoparticles. Int Nano Lett 3:30. https://doi.org/10.1186/2228-5326-3-30

18. Pourrahimi AM, Liu D, Pallon LKH, et al (2014) Water-based synthesis and cleaning methods for high purity ZnO nanoparticles-comparing acetate, chloride, sulphate and nitrate zinc salt precursors. RSC Adv 4:35568–35577. https://doi.org/10.1039/c4ra06651k

19. Devaraj NK, Han TC, Low PL, et al (2014) Synthesis and characterisation of zinc oxide nanoparticles for thermoelectric application. Mater Res Innov 18:350–353. https://doi.org/10.1179/1432891714z.000000000980

20. Top A, Çetinkaya H (2015) Zinc oxide and zinc hydroxide formation via aqueous precipitation: Effect of the preparation route and lysozyme addition. Mater Chem Phys 167:77–87. https://doi.org/10.1016/j.matchemphys.2015.10.013

21. Pelicano CM, Magdaluyo E, Ishizumi A (2016) Temperature Dependence of Structural and Optical Properties of ZnO Nanoparticles Formed by Simple Precipitation Method. In: MATEC Web of Conferences. pp 02001-1-02001–4

22. Moghri Moazzen MA, Borghei SM, Taleshi F (2013) Change in the morphology of ZnO nanoparticles upon changing the reactant concentration. Appl Nanosci 3:295–302. https://doi.org/10.1007/s13204-012-0147-z

23. Bauermann LP, Campo A Del, Bill J, Aldinger F (2006) Heterogeneous nucleation of ZnO using gelatin as the organic matrix. Chem Mater 18:2016–2020. https://doi.org/10.1021/cm052317+

24. Tseng YH, Lin HY, Liu MH, et al (2009) Biomimetic synthesis of nacrelike faceted mesocrystals of ZnO-gelatin composite. J Phys Chem C 113:18053–18061. https://doi.org/10.1021/jp905145y

25. Kang SZ, Wu T, Li X, Mu J (2010) A facile gelatin-assisted preparation and photocatalytic activity of zinc oxide nanosheets. Colloids Surfaces A Physicochem Eng Asp 369:268–271. https://doi.org/10.1016/j.colsurfa.2010.08.029

26. Guo G, Gan Y, Gu F, et al (2010) Biomimetic synthesis of zinc oxide 3D architectures with gelatin as matrix. J Nanomater 2010:1–8. https://doi.org/10.1155/2010/289173

27. Zak AK, Majid WHA, Darroudi M, Yousefi R (2011) Synthesis and characterization of ZnO nanoparticles prepared in gelatin media. Mater Lett 65:70–73. https://doi.org/10.1016/j.matlet.2010.09.029

28. Alnarabiji MS, Yahya N, Hamed Y, et al (2017) Scalable bio-friendly method for production of homogeneous metal oxide nanoparticles using green bovine skin gelatin. J Clean Prod 162:186–194. https://doi.org/10.1016/j.jclepro.2017.06.010

29. Divya M, Vaseeharan B, Abinaya M, et al (2018) Biopolymer gelatin-coated zinc oxide nanoparticles showed high antibacterial, antibiofilm and anti-angiogenic activity. J Photochem Photobiol B Biol 178:211–218. https://doi.org/10.1016/j.jphotobiol.2017.11.008

30. Pandurangan M, Kim DH (2015) In vitro toxicity of zinc oxide nanoparticles: a review. J Nanoparticle Res 17:158. https://doi.org/10.1007/s11051-015-2958-9

31. Sirelkhatim A, Mahmud S, Seeni A, et al (2015) Review on zinc oxide nanoparticles: Antibacterial activity and toxicity mechanism. Nano-Micro Lett 7:219–242. https://doi.org/10.1007/s40820-015-0040-x

32. Lallo da Silva B, Abuçafy MP, Berbel Manaia E, et al (2019) Relationship Between Structure And Antimicrobial Activity Of Zinc Oxide Nanoparticles: An Overview. Int J Nanomedicine Volume 14:9395–9410. https://doi.org/10.2147/IJN.S216204

33. Sawai J (2003) Quantitative evaluation of antibacterial activities of metallic oxide powders (ZnO, MgO and CaO) by conductimetric assay. J Microbiol Methods 54:177–182. https://doi.org/10.1016/S0167-7012(03)00037-X

34. Heidenau F, Mittelmeier W, Detsch R, et al (2005) A novel antibacterial titania coating: Metal ion toxicity and in vitro surface colonization. J Mater Sci Mater Med 16:883–888. https://doi.org/10.1007/s10856-005-4422-3

35. Brayner R, Ferrari-Iliou R, Brivois N, et al (2006) Toxicological impact studies based on Escherichia coli bacteria in ultrafine ZnO nanoparticles colloidal medium. Nano Lett 6:866–870. https://doi.org/10.1021/nl052326h

36. Franklin NM, Rogers NJ, Apte SC, et al (2007) Comparative Toxicity of Nanoparticulate ZnO, Bulk ZnO and ZnCl2 to a Freshwater Microalga (Pseudokirchneriella subcapitata): The Importance of Particle Solubility. Environ Sci Technol 41:8484–8490. https://doi.org/10.1021/es071445r

37. Huang Z, Zheng X, Yan D, et al (2008) Toxicological effect of ZnO nanoparticles based on bacteria. Langmuir 24:4140–4144. https://doi.org/10.1021/la7035949

38. Tiwari V, Mishra N, Gadani K, et al (2018) Mechanism of Anti-bacterial Activity of Zinc Oxide Nanoparticle Against Carbapenem-Resistant Acinetobacter baumannii. Front Microbiol 9:1218. https://doi.org/10.3389/fmicb.2018.01218

39. Kadiyala U, Turali-Emre ES, Bahng JH, et al (2018) Unexpected insights into antibacterial activity of zinc oxide nanoparticles against methicillin resistant: Staphylococcus aureus (MRSA). Nanoscale 10:4927–4939. https://doi.org/10.1039/c7nr08499d

40. Agarwal H, Menon S, Venkat Kumar S, Rajeshkumar S (2018) Mechanistic study on antibacterial action of zinc oxide nanoparticles synthesized using green route. Chem Biol Interact 286:60–70. https://doi.org/10.1016/j.cbi.2018.03.008

41. Dimapilis EAS, Hsu CS, Mendoza RMO, Lu MC (2018) Zinc oxide nanoparticles for water disinfection. Sustain Environ Res 28:47–56. https://doi.org/10.1016/j.serj.2017.10.001

42. Yamamoto O (2001) Influence of particle size on the antibacterial activity of zinc oxide. Int J Inorg Mater 3:643–646. https://doi.org/10.1016/S1466-6049(01)00197-0

43. Raghupathi KR, Koodali RT, Manna AC (2011) Size-dependent bacterial growth inhibition and mechanism of antibacterial activity of zinc oxide nanoparticles. Langmuir 27:4020–4028. https://doi.org/10.1021/la104825u

44. Yang H, Liu C, Yang D, et al (2009) Comparative study of cytotoxicity, oxidative stress and genotoxicity induced by four typical nanomaterials: the role of particle size, shape and composition. J Appl Toxicol 29:69–78. https://doi.org/10.1002/jat.1385

45. Dobrucka R, Długaszewska J (2016) Biosynthesis and antibacterial activity of ZnO nanoparticles using Trifolium pratense flower extract. Saudi J Biol Sci 23:517–523. https://doi.org/10.1016/j.sjbs.2015.05.016

46. Reshma VG, Mohanan PV (2017) Cellular interactions of zinc oxide nanoparticles with human embryonic kidney (HEK 293) cells. Colloids Surfaces B Biointerfaces 157:182–190. https://doi.org/10.1016/j.colsurfb.2017.05.069

47. Taghizadeh S-M, Lal N, Ebrahiminezhad A, et al (2020) Green and Economic Fabrication of Zinc Oxide (ZnO) Nanorods as a Broadband UV Blocker and Antimicrobial Agent. Nanomaterials 10:530. https://doi.org/10.3390/nano10030530

48. Leung YH, Chan CMN, Ng AMC, et al (2012) Antibacterial activity of ZnO nanoparticles with a modified surface under ambient illumination. Nanotechnology 23:475703. https://doi.org/10.1088/0957-4484/23/47/475703

49. Hsu A, Liu F, Leung YH, et al (2014) Is the effect of surface modifying molecules on antibacterial activity universal for a given material? Nanoscale 6:10323–10331. https://doi.org/10.1039/c4nr02366h

50. Arakha M, Saleem M, Mallick BC, Jha S (2015) The effects of interfacial potential on antimicrobial propensity of ZnO nanoparticle. Sci Rep 5:1–10. https://doi.org/10.1038/srep09578

51. Premanathan M, Karthikeyan K, Jeyasubramanian K, Manivannan G (2011) Selective toxicity of ZnO nanoparticles toward Gram-positive bacteria and cancer cells by apoptosis through lipid peroxidation. Nanomedicine Nanotechnology, Biol Med 7:184–192. https://doi.org/10.1016/j.nano.2010.10.001

52. Tayel AA, El-Tras WF, Moussa S, et al (2011) Antibacterial action of zinc oxide nanoparticles against foodborne pathogens. J Food Saf 31:211–218. https://doi.org/10.1111/j.1745-4565.2010.00287.x

53. Pranjali P, Meher MK, Raj R, et al (2019) Physicochemical and Antibacterial Properties of PEGylated Zinc Oxide Nanoparticles Dispersed in Peritoneal Dialysis Fluid. ACS Omega 4:19255–19264. https://doi.org/10.1021/acsomega.9b02615

54. Saliani M, Jalal R, Goharshadi EK (2015) Effects of pH and temperature on antibacterial activity of zinc oxide nanofluid against Escherichia coli O157: H7 and Staphylococcus aureus. Jundishapur J Microbiol 8:1–6. https://doi.org/10.5812/jjm.17115

55. Senapati VA, Kumar A (2018) ZnO nanoparticles dissolution, penetration and toxicity in human epidermal cells. Influence of pH. Environ Chem Lett 16:1129–1135. https://doi.org/10.1007/s10311-018-0736-5

56. Miao AJ, Zhang XY, Luo Z, et al (2010) Zinc oxide-engineered nanoparticles: Dissolution and toxicity to marine phytoplankton. Environ Toxicol Chem 29:2814–2822.

https://doi.org/10.1002/etc.340

57. Reddy KM, Feris K, Bell J, et al (2007) Selective toxicity of zinc oxide nanoparticles to prokaryotic and eukaryotic systems. Appl Phys Lett 90:213902. https://doi.org/10.1063/1.2742324

58. Hanley C, Layne J, Punnoose A, et al (2008) Preferential killing of cancer cells and activated human T cells using ZnO nanoparticles. Nanotechnology 19:295103. https://doi.org/10.1088/0957-4484/19/29/295103

59. Moratin H, Scherzad A, Gehrke T, et al (2018) Toxicological Characterization of ZnO Nanoparticles in Malignant and Non-Malignant Cells. Environ Mol Mutagen 59:247–259. https://doi.org/10.1002/em.22156

60. Holmes AM, Mackenzie L, Roberts MS (2020) Disposition and measured toxicity of zinc oxide nanoparticles and zinc ions against keratinocytes in cell culture and viable human epidermis. Nanotoxicology 14:263–274. https://doi.org/10.1080/17435390.2019.1692382

61. Ickrath P, Wagner M, Scherzad A, et al (2017) Time-Dependent Toxic and Genotoxic Effects of Zinc Oxide Nanoparticles after Long-Term and Repetitive Exposure to Human Mesenchymal Stem Cells. Int J Environ Res Public Health 14:1590. https://doi.org/10.3390/ijerph14121590

62. Singh S (2019) Zinc oxide nanoparticles impacts: cytotoxicity, genotoxicity, developmental toxicity, and neurotoxicity. Toxicol Mech Methods 29:300–311. https://doi.org/10.1080/15376516.2018.1553221

63. Xia T, Zhao Y, Sager T, et al (2011) Decreased dissolution of ZnO by iron doping yields nanoparticles with reduced toxicity in the rodent lung and zebrafish embryos. ACS Nano 5:1223–1235. https://doi.org/10.1021/nn1028482

64. Yin H, Casey PS (2014) Effects of iron or manganese doping of ZnO nanoparticles on their dissolution, ROS generation and cytotoxicity. RSC Adv 4:26149–26157. https://doi.org/10.1039/c4ra02481h

65. Sotiriou GA, Watson C, Murdaugh KM, et al (2014) Engineering safer-by-design silica-coated ZnO nanorods with reduced DNA damage potential. Environ Sci Nano 1:144–153. https://doi.org/10.1039/c3en00062a

66. Chia SL, Leong DT (2016) Reducing ZnO nanoparticles toxicity through silica coating. Heliyon 2:e00177. https://doi.org/10.1016/j.heliyon.2016.e00177

67. Yin H, Casey PS, McCall MJ, Fenech M (2010) Effects of Surface Chemistry on Cytotoxicity, Genotoxicity, and the Generation of Reactive Oxygen Species Induced by ZnO Nanoparticles. Langmuir 26:15399–15408. https://doi.org/10.1021/la101033n

68. Ansari SA, Husain Q, Qayyum S, Azam A (2011) Designing and surface modification of zinc oxide nanoparticles for biomedical applications. Food Chem Toxicol 49:2107–2115. https://doi.org/10.1016/j.fct.2011.05.025

69. Luo M, Shen C, Feltis BN, et al (2014) Reducing ZnO nanoparticle cytotoxicity by surface modification. Nanoscale 6:5791–5798. https://doi.org/10.1039/c4nr00458b

70. Altunbek M, Baysal A, Çulha M (2014) Influence of surface properties of zinc oxide nanoparticles on their cytotoxicity. Colloids Surfaces B Biointerfaces 121:106–113. https://doi.org/10.1016/j.colsurfb.2014.05.034

71. Yin H, Chen R, Casey PS, et al (2015) Reducing the cytotoxicity of ZnO nanoparticles by a pre-formed protein corona in a supplemented cell culture medium. RSC Adv 5:73963–73973. https://doi.org/10.1039/c5ra14870g

72. Wolska-Pietkiewicz M, Tokarska K, Grala A, et al (2018) Safe-by-Design Ligand-Coated ZnO Nanocrystals Engineered by an Organometallic Approach: Unique Physicochemical Properties and Low Toxicity toward Lung Cells. Chem - A Eur J 24:4033–4042. https://doi.org/10.1002/chem.201704207

73. Kraegeloh A, Suarez-Merino B, Sluijters T, Micheletti C (2018) Implementation of Safe-by-Design for Nanomaterial Development and Safe Innovation: Why We Need a Comprehensive Approach.

Nanomaterials 8:239. https://doi.org/10.3390/nano8040239

74. Lin S, Yu T, Yu Z, et al (2018) Nanomaterials Safer-by-Design: An Environmental Safety Perspective. Adv Mater 30:1–5. https://doi.org/10.1002/adma.201705691

75. Ferrone E, Araneo R, Notargiacomo A, et al (2019) ZnO Nanostructures and Electrospun ZnO–Polymeric Hybrid Nanomaterials in Biomedical, Health, and Sustainability Applications. Nanomaterials 9:1449. https://doi.org/10.3390/nano9101449

76. Osseni R., Debbasch C, Christen M-O, et al (1999) Tacrine-induced Reactive Oxygen Species in a Human Liver Cell Line: The Role of Anethole Dithiolethione as a Scavenger. Toxicol Vitr 13:683–688. https://doi.org/10.1016/S0887-2333(99)00050-8

77. Petković J, Žegura B, Stevanović M, et al (2011) DNA damage and alterations in expression of DNA damage responsive genes induced by TiO2 nanoparticles in human hepatoma HepG2 cells. Nanotoxicology 5:341–353. https://doi.org/10.3109/17435390.2010.507316

78. Singh NP, McCoy MT, Tice RR, Schneider EL (1988) A simple technique for quantitation of low levels of DNA damage in individual cells. Exp Cell Res 175:184–191. https://doi.org/10.1016/0014-4827(88)90265-0

79. Møller P, Azqueta A, Boutet-Robinet E, et al (2020) Minimum Information for Reporting on the Comet Assay (MIRCA): recommendations for describing comet assay procedures and results. Nat. Protoc. 15:3817–3826

80. Zhou J, Zhao F, Wang Y, et al (2007) Size-controlled synthesis of ZnO nanoparticles and their photoluminescence properties. J Lumin 122–123:195–197. https://doi.org/10.1016/j.jlumin.2006.01.089

81. Barros BS, Barbosa R, dos Santos NR, et al (2006) Synthesis and x-ray diffraction characterization of nanocrystalline ZnO obtained by Pechini method. Inorg Mater 42:1348–1351. https://doi.org/10.1134/S0020168506120119

82. Khan MF, Ansari AH, Hameedullah M, et al (2016) Sol-gel synthesis of thorn-like ZnO nanoparticles endorsing mechanical stirring effect and their antimicrobial activities: Potential role as nano-antibiotics. Sci Rep 6:1–12. https://doi.org/10.1038/srep27689

83. Kong J, Yu S (2007) Fourier transform infrared spectroscopic analysis of protein secondary structures. Acta Biochim Biophys Sin (Shanghai) 39:549–559. https://doi.org/10.1111/j.1745-7270.2007.00320.x

84. Jackson M, Choo L-P, Watson PH, et al (1995) Beware of connective tissue proteins: Assignment and implications of collagen absorptions in infrared spectra of human tissues. Biochim Biophys Acta - Mol Basis Dis 1270:1–6. https://doi.org/10.1016/0925-4439(94)00056-V

85. Segneanu AE, Gozescu I, Dabici A, et al (2012) Organic Compounds FT-IR Spectroscopy. In: Uddin J (ed) Macro To Nano Spectroscopy. IntechOpen, pp 145–164

86. Nindiyasari F, Fernández-Díaz L, Griesshaber E, et al (2014) Influence of gelatin hydrogel porosity on the crystallization of CaCO3. Cryst Growth Des 14:1531–1542. https://doi.org/10.1021/cg401056t

87. Ebrahiminezhad A, Moeeni F, Taghizadeh S-M, et al (2019) Xanthan Gum Capped ZnO Microstars as a Promising Dietary Zinc Supplementation. Foods 8:88. https://doi.org/10.3390/foods8030088

88. Gupta M, Tomar RS, Kaushik S, et al (2018) Effective antimicrobial activity of green ZnO nano particles of Catharanthus roseus. Front Microbiol 9:2030. https://doi.org/10.3389/fmicb.2018.02030

89. Umamaheswari A, Prabu SL, John SA, Puratchikody A (2021) Green synthesis of zinc oxide nanoparticles using leaf extracts of Raphanus sativus var. Longipinnatus and evaluation of their anticancer property in A549 cell lines. Biotechnol Reports 29:e00595. https://doi.org/10.1016/j.btre.2021.e00595

90. Kumar A, Dixit CK (2017) Methods for characterization of nanoparticles. In: Advances in Nanomedicine for the Delivery of Therapeutic Nucleic Acids. Elsevier Inc., pp 44–58

91. Kim KM, Choi MH, Lee JK, et al (2014) Physicochemical properties of surface charge-modified ZnO

nanoparticles with different particle sizes. Int J Nanomedicine 9:41–56. https://doi.org/10.2147/IJN.S57923

92. Reed RB, Ladner DA, Higgins CP, et al (2012) Solubility of nano-zinc oxide in environmentally and biologically important matrices. Environ Toxicol Chem 31:93–99. https://doi.org/10.1002/etc.708

93. Corbo C, Molinaro R, Parodi A, et al (2016) The impact of nanoparticle protein corona on cytotoxicity, immunotoxicity and target drug delivery. Nanomedicine 11:81–100

94. Baimanov D, Cai R, Chen C (2019) Understanding the Chemical Nature of Nanoparticle–Protein Interactions. Bioconjug Chem 30:1923–1937. https://doi.org/10.1021/acs.bioconjchem.9b00348

95. Kulkarni VS, Shaw C (2016) Use of Polymers and Thickeners in Semisolid and Liquid Formulations. In: Essential Chemistry for Formulators of Semisolid and Liquid Dosages. Elsevier, pp 43–69

96. Bandeira M, Giovanela M, Roesch-Ely M, et al (2020) Green synthesis of zinc oxide nanoparticles: A review of the synthesis methodology and mechanism of formation. Sustain. Chem. Pharm. 15:100223

97. Bressac B, Galvin KM, Liang TJ, et al (1990) Abnormal structure and expression of p53 gene in human hepatocellular carcinoma. Proc Natl Acad Sci U S A 87:1973–1977. https://doi.org/10.1073/pnas.87.5.1973

98. Waldherr M, Mišík M, Ferk F, et al (2018) Use of HuH6 and other human-derived hepatoma lines for the detection of genotoxins: a new hope for laboratory animals? Arch Toxicol 92:921–934. https://doi.org/10.1007/s00204-017-2109-4

99. Westerink WMA, Schoonen WGEJ (2007) Cytochrome P450 enzyme levels in HepG2 cells and cryopreserved primary human hepatocytes and their induction in HepG2 cells. Toxicol Vitr 21:1581–1591. https://doi.org/10.1016/j.tiv.2007.05.014

100. Sharma V, Anderson D, Dhawan A (2012) Zinc oxide nanoparticles induce oxidative DNA damage and ROS-triggered mitochondria mediated apoptosis in human liver cells (HepG2). Apoptosis 17:852–870. https://doi.org/10.1007/s10495-012-0705-6

101. Sliwinska A, Kwiatkowski D, Czarny P, et al (2015) Genotoxicity and cytotoxicity of ZnO and Al2O3 nanoparticles. Toxicol Mech Methods 25:176–183. https://doi.org/10.3109/15376516.2015.1006509

102. Hackenberg S, Zimmermann F-Z, Scherzed A, et al (2011) Repetitive exposure to zinc oxide nanoparticles induces dna damage in human nasal mucosa mini organ cultures. Environ Mol Mutagen 52:582–589. https://doi.org/10.1002/em.20661

103. Hackenberg S, Scherzed A, Zapp A, et al (2017) Genotoxic effects of zinc oxide nanoparticles in nasal mucosa cells are antagonized by titanium dioxide nanoparticles. Mutat Res Toxicol Environ Mutagen 816–817:32–37. https://doi.org/10.1016/j.mrgentox.2017.02.005

104. El Yamani N, Collins AR, Rundén-Pran E, et al (2017) *In vitro* genotoxicity testing of four reference metal nanomaterials, titanium dioxide, zinc oxide, cerium oxide and silver: towards reliable hazard assessment. Mutagenesis 32:117–126. https://doi.org/10.1093/mutage/gew060

105. Wahab R, Siddiqui MA, Saquib Q, et al (2014) ZnO nanoparticles induced oxidative stress and apoptosis in HepG2 and MCF-7 cancer cells and their antibacterial activity. Colloids Surfaces B Biointerfaces 117:267–276. https://doi.org/10.1016/j.colsurfb.2014.02.038

106. Sahu D, Kannan GM, Tailang M, Vijayaraghavan R (2016) *In Vitro* Cytotoxicity of Nanoparticles: A Comparison between Particle Size and Cell Type. J Nanosci 2016:1–9. https://doi.org/10.1155/2016/4023852

107. Zijno A, De Angelis I, De Berardis B, et al (2015) Different mechanisms are involved in oxidative DNA damage and genotoxicity induction by ZnO and TiO2 nanoparticles in human colon carcinoma cells. Toxicol Vitr 29:1503–1512. https://doi.org/10.1016/j.tiv.2015.06.009

108. Xiao L, Liu C, Chen X, Yang Z (2016) Zinc oxide nanoparticles induce renal toxicity through reactive oxygen species. Food Chem Toxicol 90:76–83. https://doi.org/10.1016/j.fct.2016.02.002

109. Roy Choudhury S, Ordaz J, Lo C-L, et al (2017) Zinc oxide Nanoparticles-Induced Reactive Oxygen Species Promotes Multimodal Cyto- and Epigenetic Toxicity. Toxicol Sci 156:261–274.

https://doi.org/10.1093/toxsci/kfw252

110. Xia T, Kovochich M, Liong M, et al (2008) Comparison of the Mechanism of Toxicity of Zinc Oxide and Cerium Oxide Nanoparticles Based on Dissolution and Oxidative Stress Properties. ACS Nano 2:2121–2134. https://doi.org/10.1021/nn800511k

Figure captions

Fig. 1 Thermograms of GM ZnO NP powders before calcination: (**a**) TG curves and (**b**) DTA curves of GM ZnO NP powders synthesized at the surface of hydrogels with different gelatin content (ZnO-5, ZnO-10, and ZnO-15)

Fig. 2 XRD of the GM ZnO NP powders synthesized at the surface of hydrogels with different gelatin content (ZnO-5, ZnO-10, and ZnO-15)

Fig. 3 SEM images of the GM ZnO NP powders synthesized at the surface of hydrogels with different gelatin content (ZnO-5 (**a**, **b, c**), ZnO-10 (**d, e, f**), and ZnO-15 (**g, h, i**))

Fig. 4 FTIR-ATR spectra of (**a**) pure gelatin film with 10 wt% of gelatin content (Gel 10 wt%) and (**b**) GM ZnO NP powders synthesized at the surface of hydrogels with different gelatin content (ZnO-5, ZnO-10, and ZnO-15)

Fig. 5 The viability of HepG2 cells treated with GM ZnO NPs (0.01, 0.1, 1, 10, and 100 μg mL^{-1}) for 24 h: (**a**) ZnO-5, (**b**) ZnO-10, and (**c**) ZnO-15. The asterisks denote a significant difference between solvent control and treated cells (*$P < 0.05$; ** $P < 0.05$; ***$P < 0.001$). The line denotes 25% decrease of cell viability. Positive control (PC): 125 μg mL^{-1} ET. The data are presented as mean values ± standard deviation

Fig. 6 Induction of ROS formation by GM ZnO NPs ((**a**) ZnO-5, (**b**) ZnO-10, and (**c**) ZnO-15) in HepG2 cells. The HepG2 cells were pretreated with DCFH-DA (20 μmol L^{-1}) for 30 min and then exposed to different concentrations of NPs (0.1, 1, 10, and 100 μg mL^{-1}). TBHP (0.5 mmol L^{-1}) was used as the positive control (PC). DCF fluorescence intensity was measured at 30 min intervals for 150 min. The data are presented as mean values ± standard deviation

Fig. 7 DNA damage induced by GM ZnO NPs in HepG2 cells. Cells were exposed to (**a**) ZnO-5, (**b**) ZnO-10, and (**c**) ZnO-15 GM ZnO NPs (0.1, 1, 10, and 100 μg mL^{-1}) for 24 h. BaP (30 μmol L^{-1}) was used as a positive control (PC). The DNA damage was assessed with the alkaline comet assay and is expressed as a percentage of tail DNA. Fifty cells were analyzed per experimental point in each of the three independent experiments. Data are presented as quantile box plots. The edges of the box represent the 25th and 75th percentiles; the median is a solid line through the box, and the 95% confidence intervals are shown. Significant difference (one-way ANOVA; Dunnett's Multiple Comparison test) between NP-exposed cells and the solvent control (0) is indicated by ***$P < 0.001$, and ****$P < 0.0001$

Programs used to create the artwork

Fig. 1: MATLAB R2016b, Inkscape 1.0.1, GIMP 2.8.20

Fig. 2: MATLAB R2016b, Inkscape 1.0.1, GIMP 2.8.20

Fig. 3: MATLAB R2016b, Inkscape 1.0.1, GIMP 2.8.20

Fig. 4: MATLAB R2016b, Inkscape 1.0.1, GIMP 2.8.20

Fig. 5: GraphPad Prism V6, Inkscape 1.0.1, GIMP 2.8.20

Fig. 6: GraphPad Prism V6, Inkscape 1.0.1, GIMP 2.8.20

Fig. 7: GraphPad Prism V6, Inkscape 1.0.1, GIMP 2.8.20

Fig. 1

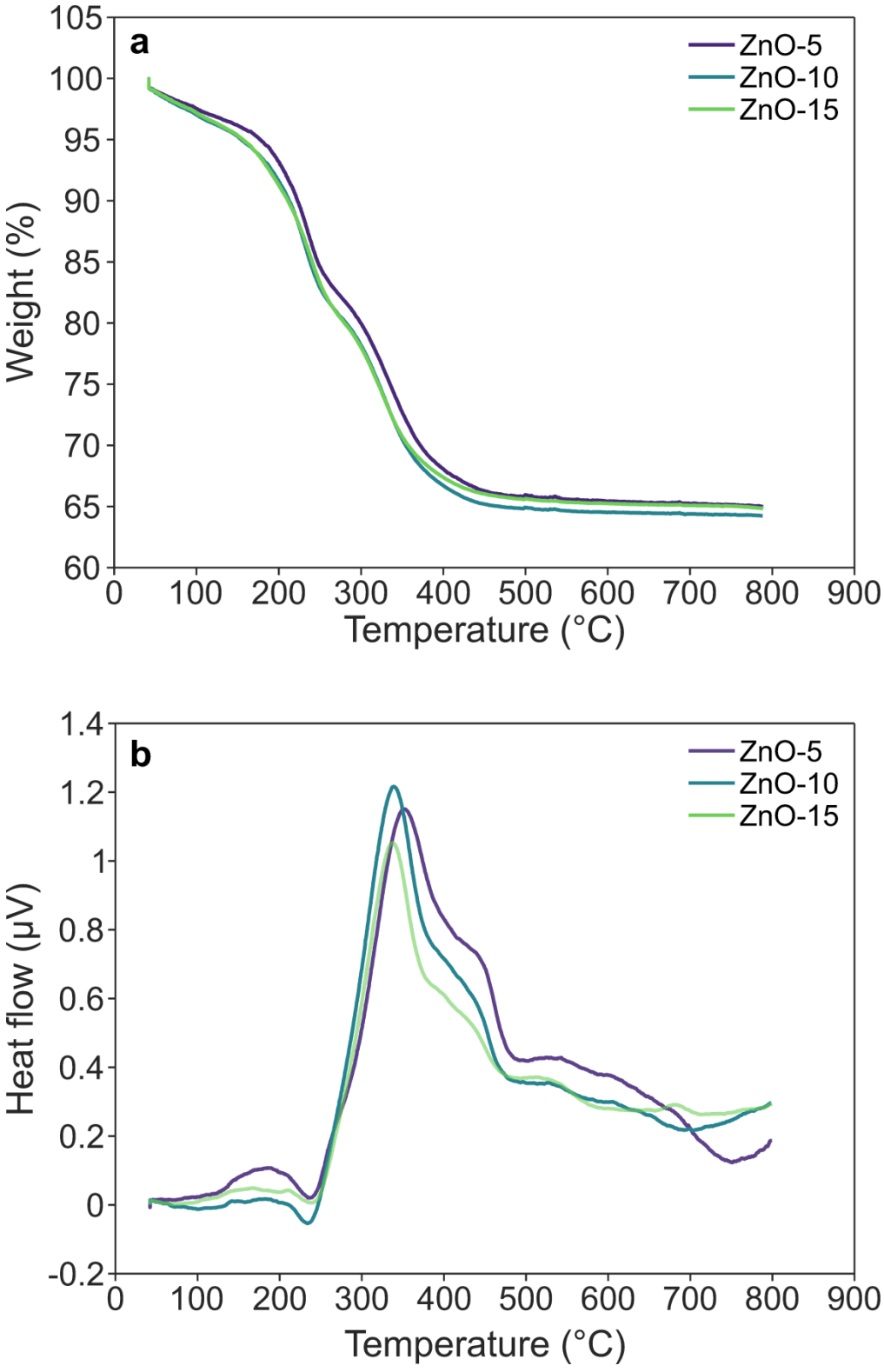
a
ZnO-5
ZnO-10
ZnO-15
Weight (%)
105
100
95
90
85
80
75
70
65
60
0
100
200
300
400
500
600
700
800
900
Temperature (°C)
b
ZnO-5
ZnO-10
ZnO-15
Heat flow (μV)
1.4
1.2
1
0.8
0.6
0.4
0.2
0
-0.2
0
100
200
300
400
500
600
700
800
900
Temperature (°C)

Fig. 2

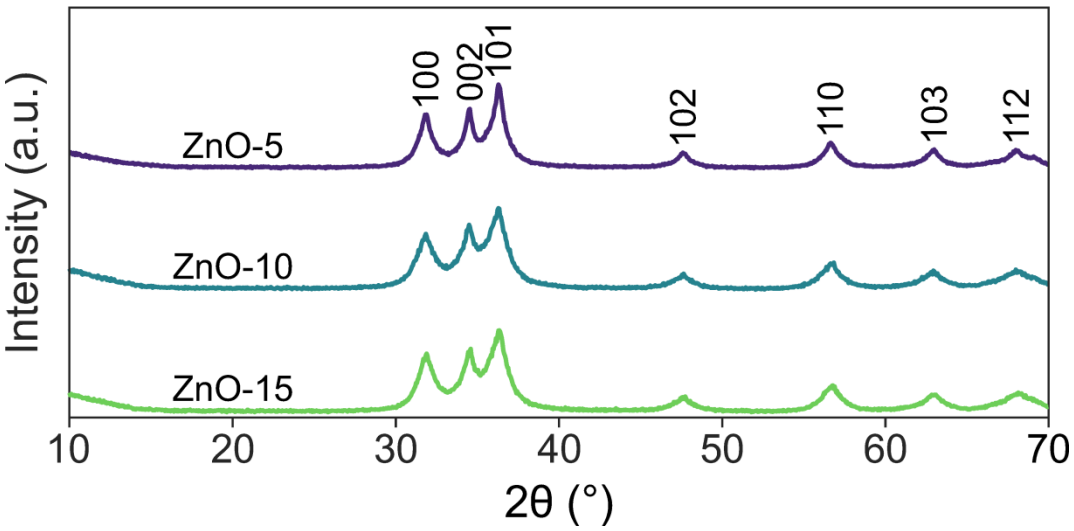
Intensity (a.u.)
100
002
101
102
110
103
112
ZnO-5
ZnO-10
ZnO-15
10
20
30
40
50
60
70
2θ (°)

Fig. 3

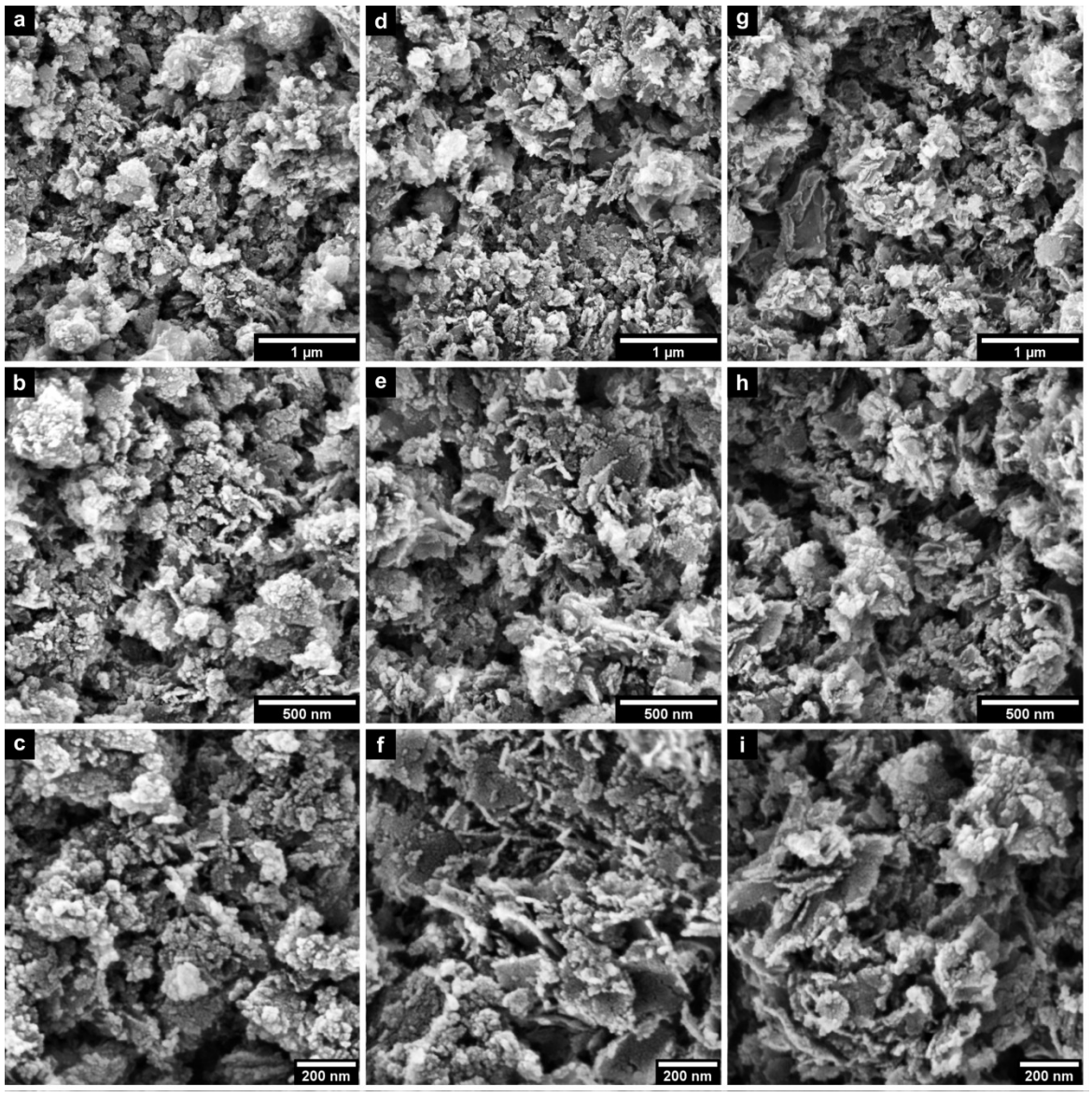
a
1 µm
d
1 µm
g
1 µm
b
500 nm
e
500 nm
h
500 nm
c
200 nm
f
200 nm
i
200 nm

Fig. 4

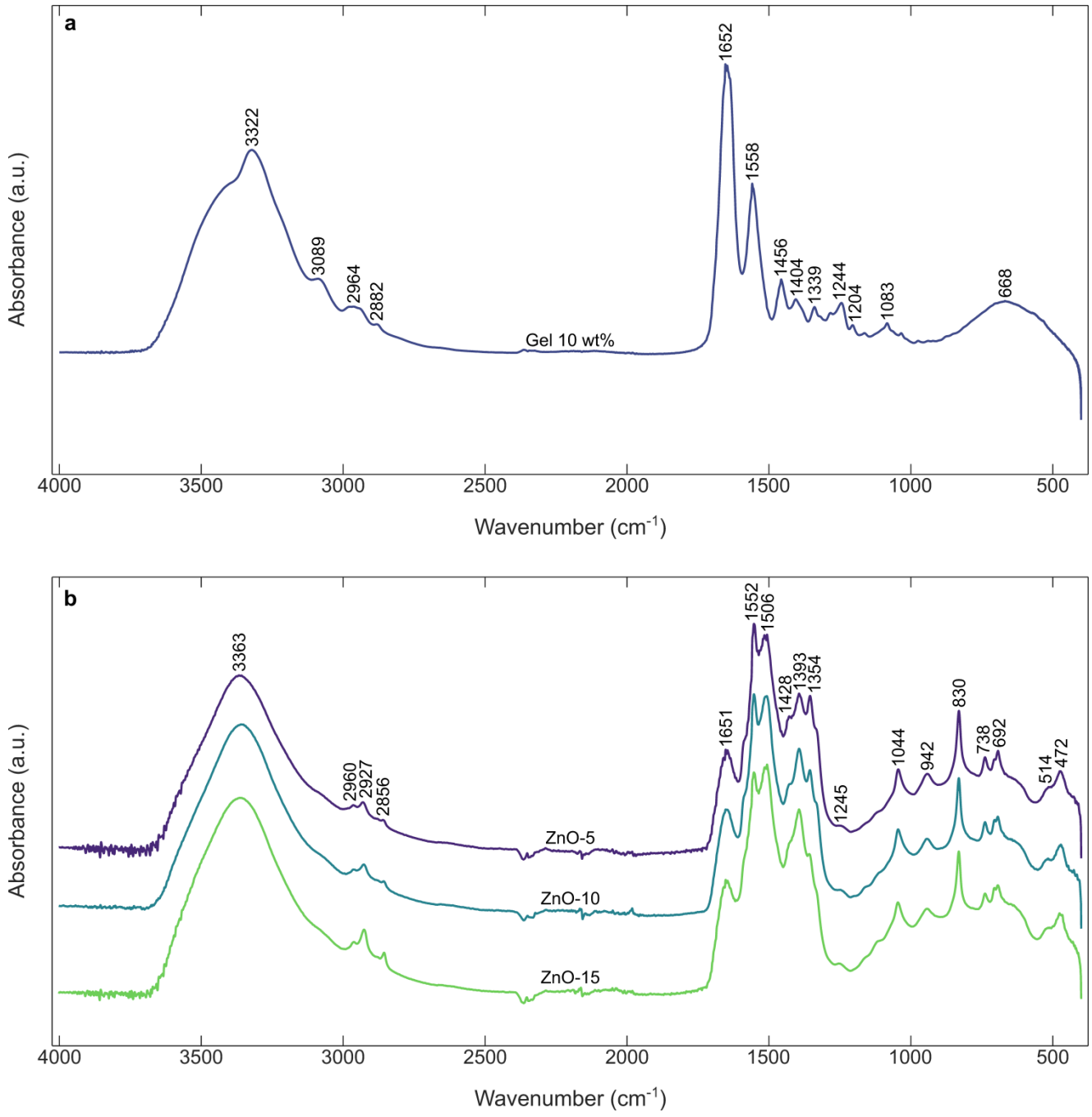
a
Absorbance (a.u.)
3322
3089
2964
2882
1652
1558
1456
1404
1339
1244
1204
1083
668
Gel 10 wt%
4000
3500
3000
2500
2000
1500
1000
500
Wavenumber (cm-1)
b
Absorbance (a.u.)
3363
2960
2927
2856
1651
1552
1506
1428
1393
1354
1245
1044
942
830
738
692
514
472
ZnO-5
ZnO-10
ZnO-15
4000
3500
3000
2500
2000
1500
1000
500
Wavenumber (cm-1)

Fig. 5

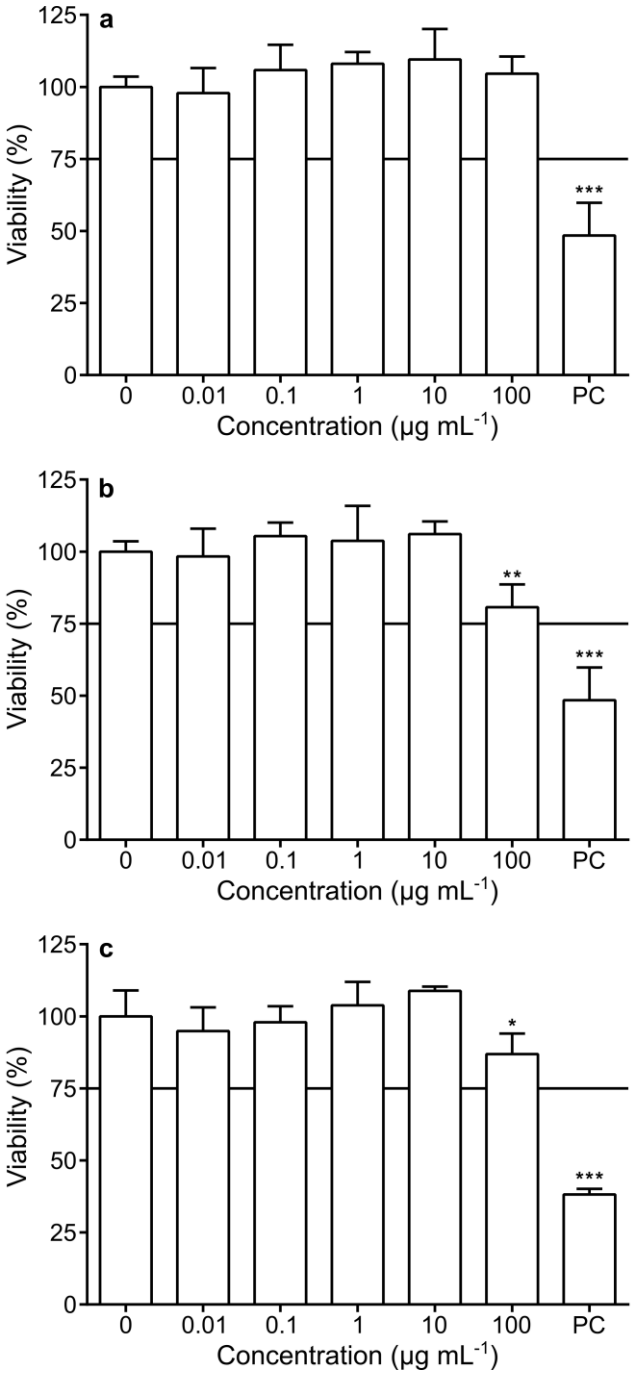
a
b
c
Viability (%)
125
100
75
50
25
0
***
**
*
0
0.01
0.1
1
10
100
PC
Concentration (μg mL-1)

Fig. 6

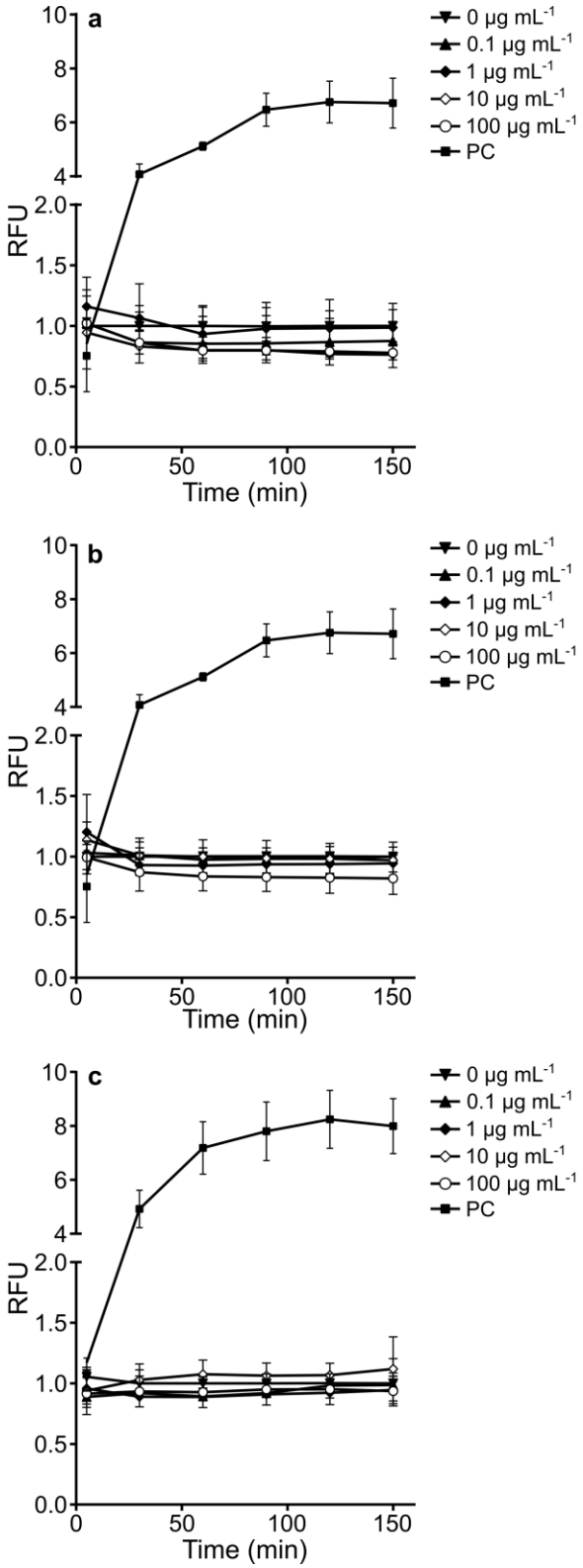

Fig. 7

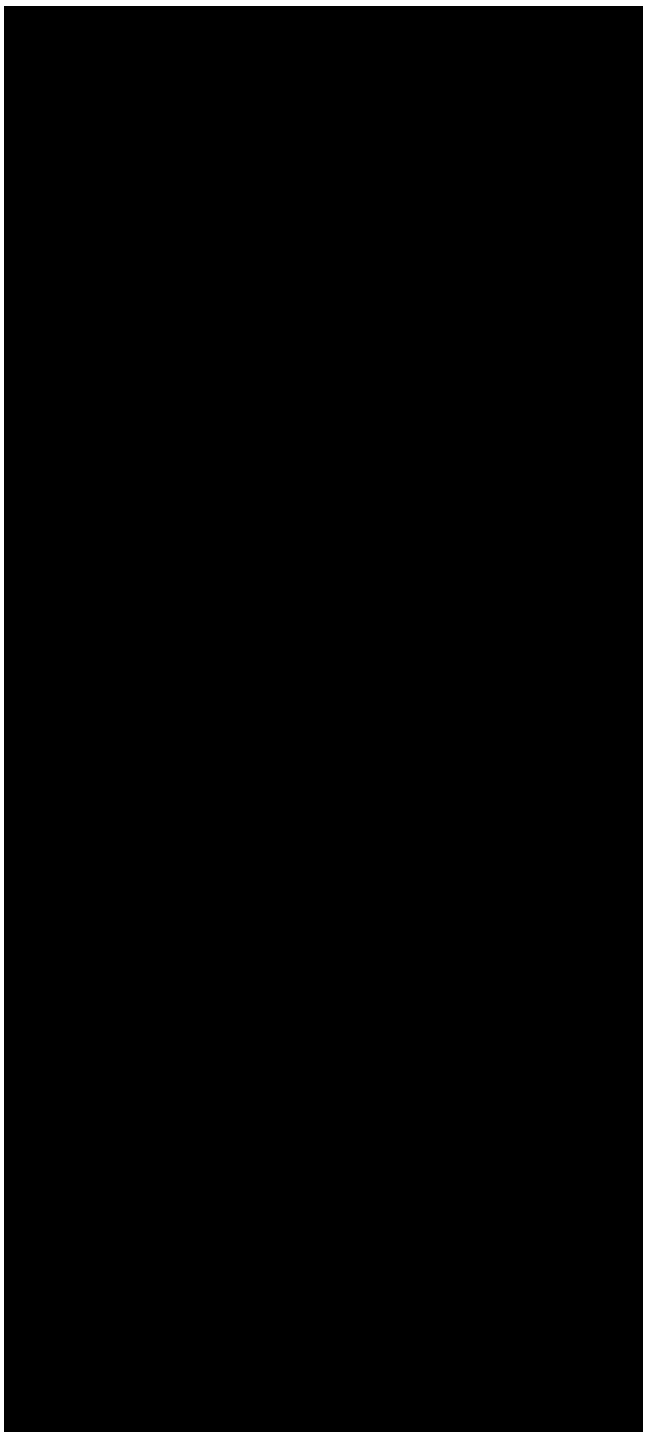

Graphical abstract